Catalysis Today 170 (2011) 69–75

Contents lists available at ScienceDirect

Catalysis Today

journal homepage: www.elsevier.com/locate/cattod

Quasi in situ Mössbauer and XAS studies on FeB nanoalloy for heterogeneous catalytic dehydrogenation of ammonia borane

Teng He[a,b], Junhu Wang[a], Tao Liu[c], Guotao Wu[a], Zhitao Xiong[a], Jie Yin[a,b], Hailiang Chu[a], Tao Zhang[a], Ping Chen[a,*]

[a] Dalian Institute of Chemical Physics, Chinese Academy of Sciences, 116023 Dalian, China
[b] Graduate University of Chinese Academy of Sciences, 100049 Beijing, China
[c] Institute for Synchrotron Radiation, Karlsruhe Institute of Technology, 76344, Germany

ARTICLE INFO

Article history:
Received 29 August 2010
Received in revised form 17 February 2011
Accepted 21 February 2011
Available online 3 April 2011

Keywords:
Ammonia borane
Hydrogen storage
Heterogeneous catalysis
Fe–B nanoalloy
Mössbauer
XAS

ABSTRACT

In our previous report, about 1 equiv. H_2 can be evolved from a Fe-modified ammonia borane (AB) sample at a temperature as low as 60 °C with significant depression of induction period, sample foaming and toxic byproducts [1]. In this study, the effects of catalyst precursors and catalyst loading were investigated on the hydrogen desorption profile and the formation of crystalline polyaminoborane (PAB). The experimental results show that loading 2.0 mol.% $FeCl_3$ to solid-state AB gives the best performance of formation of crystalline PAB. The rate of hydrogen evolution from the Fe-modified AB is 5.8 times as that of neat AB at 60 °C. X-ray absorption spectroscopy (XAS) and quasi in situ ^{57}Fe Mössbauer characterizations show that Fe–B nanoalloy, which functions as catalytic species in the dehydrogenation, is formed upon mixing AB with $FeCl_3$.

1. Introduction

Onboard hydrogen storage is a key technology of the hydrogen-based energy system [2,3]. AB (NH_3BH_3) with a hydrogen content of 19.6 wt.% has attracted increasing attention as a promising hydrogen storage material [4,5]. Dehydrogenation of AB is a three-step process, releasing 1 equiv. H_2 at each step. In the first two steps, about 2 equiv. H_2 evolve at temperatures higher than 100 °C due to the relatively high dehydrogenation kinetic barrier [6–8]. Thus, improving the rate of dehydrogenation is one of the challenges in its practical usage. Other drawbacks including toxic byproducts (borazine, NH_3, etc.) and sample foaming during H_2 desorption are still pending issues. In the past several years, various approaches including the uses of supports [9–11], homogeneous catalysis [12–16], ionic liquid [17,18] and chemical alternations [19–26] have been investigated widely. However, additional weight from support or solvent inevitably scarifies the hydrogen content of the system. In this context, the direct catalytic modification of solid phase AB is viewed as an attractive mean. Recently, we reported nanosized Co-, Ni- [27] and Fe–Based [1] catalysts on the heterogeneous catalytic dehydrogenation of AB and achieved approximately 1 equiv. H_2 desorption from the catalyst-doped samples at a temperature as low as 60 °C with significantly depression of sample foaming and byproducts (borazine and NH_3). Crystalline PAB is the main solid product. Metal-B alloys were identified as functional species by X-ray atomic pair distribution functions (PDFs). In this paper, quasi in situ ^{57}Fe Mössbauer and XAS techniques are employed to identify the changes of Fe chemical environment in the iron chloride modified AB during dehydrogenation process. The precursor effect (i.e. Fe with different chemical valences) and loading effect on the dehydrogenation profile and formation of crystalline PAB are also investigated. Kinetic analysis shows a reduced kinetic barrier (E_a) for releasing H_2 from the Fe-modified AB samples compared with neat one.

2. Experimental

2.1. Sample preparation

AB (Sigma–Aldrich, 97.0%), $FeCl_2$ (Sigma–Aldrich 97.0%), $FeCl_3$ (Sigma–Aldrich, 98.0%), and tetrahydrofuran (THF; 99.8% J&K Chemical) were used without further purification. 2.0, 5.0, 8.0 and 10.0 mol.% $FeCl_2$ or $FeCl_3$ were introduced into solid AB using "co-precipitation" method developed elsewhere [27]. The

* Corresponding author. Tel.: +86 411 84379905; fax: +86 411 84685940.
E-mail address: pchen@dicp.ac.cn (P. Chen).

0920-5861/$ – see front matter.
doi:10.1016/j.cattod.2011.02.041

catalyst-doped AB samples were preserved below 10 °C to avoid self-decomposition. All sample handlings were conducted in an MBraun 200 glove box filled with purified argon.

2.2. Characterizations

The decomposition of samples was investigated by a homemade temperature programmed desorption-mass spectrometer (TPD-MS) combined system with a heating rate of 1 °C min^{-1}. Volumetric release for quantitative measurements of hydrogen evolution from samples was carried out on a homemade Sievert type apparatus. Kissinger approach was adopted to obtain kinetic data, where peak temperatures at heating rates of 0.5, 1, 2 and 3 °C min^{-1} were collected on a differential scanning calorimeter (DSC) system (STA449C Netzsch Company). X-ray diffraction (XRD) measurements were conducted on a PANalytical X'pert diffractometer (Cu Kα, 40 kV, 40 mA). In order to avoid sample contamination by air, the sample holder was covered by a piece of shielding kapton film. The gaseous products were introduced into a diluted sulphuric acid to detect the NH_3 concentration from the change of conductivity of the acid solution. Fourier transform infrared (FTIR) measurements were performed on a Varian 3100 unit in transmittance mode.

Quasi in situ ^{57}Fe Mössbauer spectra were recorded at room temperature using a Topologic 500A spectrometer with a proportional counter. ^{57}Co(Rh) moving in a constant acceleration mode was used as the radioactive source. The Doppler velocity of the spectrometer was calibrated with respect to α-Fe foil. Samples were protected under Ar atmosphere during Mössbauer measurements. In the spectral analysis, the component of alloyed state iron was fitted by assuming a distribution in magnetic hyperfine field and the quadrupole splitting was negligible; the other components were fitted by assuming Lorentzian lineshapes. In this way, Mössbauer parameters such as the isomer shift (IS), the electric quadrupole splitting (QS), the full line width at half-maximum (FWHM), the magnetic hyperfine field (H), and the relative resonance areas of the different components of the absorption patterns (RI) were determined.

Room temperature XAS spectra at Fe K-edge were collected in transmission mode at BL14W1 beamline of Shanghai Synchrotron Radiation Facility (SSRF). Samples were pressed into a pellet under a pressure of 1.0 ton and coated with a kapton film bag. Metallic Fe foil, $FeCl_2$ and $FeCl_3$ were also measured as standard references and for energy calibration. Analysis of extended X-ray adsorption fine structure (EXAFS) data followed the standard procedures using WinXAS code [28]. After background removal and normalization, the XAS function in the range 2.0–10.5 Å^{-1} in k space was extracted and Fourier transform was carried out with k^2 weighting to obtain structural information around the absorbing Fe atoms.

3. Results and discussion

3.1. Precursor effect

$FeCl_2$ and $FeCl_3$ were used as catalyst precursors and introduced to AB via the "co-precipitation" method developed elsewhere [27]. Fig. 1 shows the TPD curves of the 2.0 mol.% catalysts-doped and neat AB. Identical to what reported in the literature [7,8], the first equivalent H_2 is released at peak temperature 108 °C for neat AB. While the $FeCl_2$- and $FeCl_3$-doped AB start to evolve hydrogen at around 55 °C (see Supplementary data) and give broad peaks centered at 101 and 98 °C, respectively. The second desorption peaks of the catalyst-doped AB samples are broader than that of the neat AB, indicating the formation of different types of PAB in the first

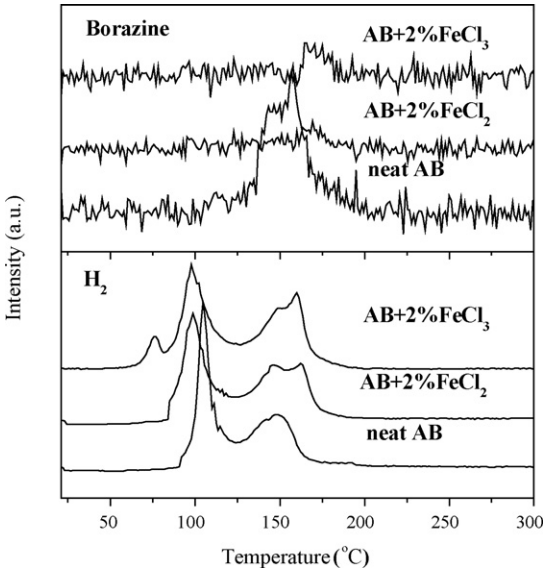

Fig. 1. TPD-MS H_2 (bottom) and borazine (top) signals of neat, 2.0 mol.% $FeCl_2$- and $FeCl_3$-doped AB samples.

desorption step, which is similar to the Co- or Ni-based catalytic dehydrogenation of AB [27]. Because of low loading of catalyst (2.0 mol.%) and the ramping of temperature, some of the AB in poor contact of catalyst may undergo self-decomposition. Therefore, the solid product of the first step of the TPD treatment may be comprised of amorphous (from self-decomposition of AB) and crystalline (from catalytic dehydrogenation of AB) PAB. Also shown in Fig. 1, borazine which is a poison product to fuel cell is significantly suppressed. Isothermal volumetric release measurements on the doped and neat AB samples (shown in Fig. 2) reveal that little H_2 is released from the neat AB at 60 °C even holding the temperature for 40 h, which is probably due to extremely long induction period [29,30]. Under the same condition, the Fe-doped AB samples evolve hydrogen immediately upon reaching the temperature showing clear difference from the diammoniate of diborane (DADB in short) initiated sigmoidal kinetic behavior of neat AB reported in the literature [29–31]. By comparison, the $FeCl_3$-doped AB sample exhibits superior performance than $FeCl_2$, i.e. the higher activity and exact evolution of 1.0 equiv. H_2. The kinetic analysis results shown in Section 3.3. Table 1 present that the specific rate constant k of $FeCl_3$-doped AB at 60 °C is 2.5 times as that of $FeCl_2$-doped AB, which is consistent with the volumetric release measure-

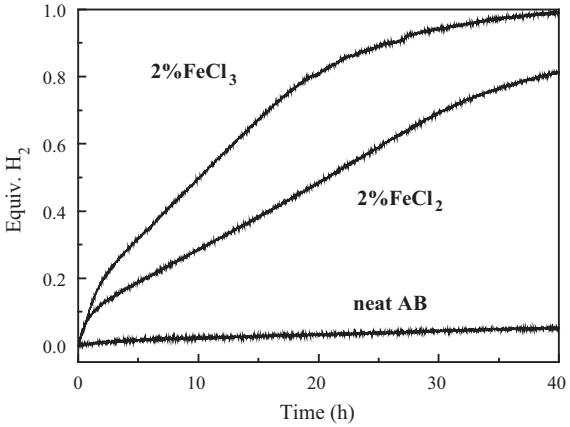

Fig. 2. Volumetric release measurements on neat, 2.0 mol.% $FeCl_2$- and $FeCl_3$-doped AB at 60 °C.

Table 1
E_a, A and k (at 60 °C) calculated from Kissinger equation and Arrhenius equation.

	E_a (kJ mol^{-1})	A (min^{-1})	k (min^{-1})
Neat AB	124.9	2.64×10^{16}	6.75×10^{-4}
AB + 2.0%$FeCl_2$	118.9	6.97×10^{15}	1.56×10^{-3}
AB + 2.0%$FeCl_3$	98.8	1.23×10^{13}	3.90×10^{-3}

ments. Noting the lower solubility of $FeCl_2$ in THF, $FeCl_2$ cannot be finely dispersed on AB during "co-precipitation". ^{57}Fe Mössbauer characterizations in Section 3.4 show that 67% $FeCl_2$ remains unchanged in the as-prepared $FeCl_2$-doped AB sample, also indicating poor dispersion of $FeCl_2$ on AB. On the contrary, due to the good solubility of $FeCl_3$ in THF, all the $FeCl_3$ can contact with AB molecules upon mixing AB with $FeCl_3$ during "co-precipitation", which is consistent with Mössbauer spectrum of as-prepared $FeCl_3$-doped AB sample. The better contacting between $FeCl_3$ and AB, i.e. better dispersion of $FeCl_3$ on AB, is responsible for the higher activity of $FeCl_3$-based catalyst. Further more, NH_3 and sample foaming were also depressed in the post-dehydrogenated AB with only 2.0 mol.% Fe loading, which agrees with the previously work [1].

3.2. Loading effect

Volumetric release measurements are carried out on AB doped with various $FeCl_2$ and $FeCl_3$ loadings at 60 °C. Normally, higher catalyst loading exhibits higher dehydrogenation rate as shown in Fig. 3. XRD is employed to identify the dehydrogenation products from neat AB at 80 °C and AB doped with various Fe loadings at 60 °C as shown in Fig. 4. The post-dehydrogenated AB sample is essentially amorphous in nature with a broad peak around 19° (Fig. 4a). However, for the Fe-doped AB samples, a strong diffraction peak at ca. 23.5° and several weak peaks at ca. 20.3°, 30.2° and 40.2° can be detected (Fig. 4b). This XRD patterns may be assignable to cyclopentaborazane (CPB $(NH_2BH_2)_5$) by Böddeker et al. [32] or Goldberg et al. [12,33], or may be a more ordered linear PAB $(NH_2BH_2)_n$ assigned by Staubitz et al. recently [34].

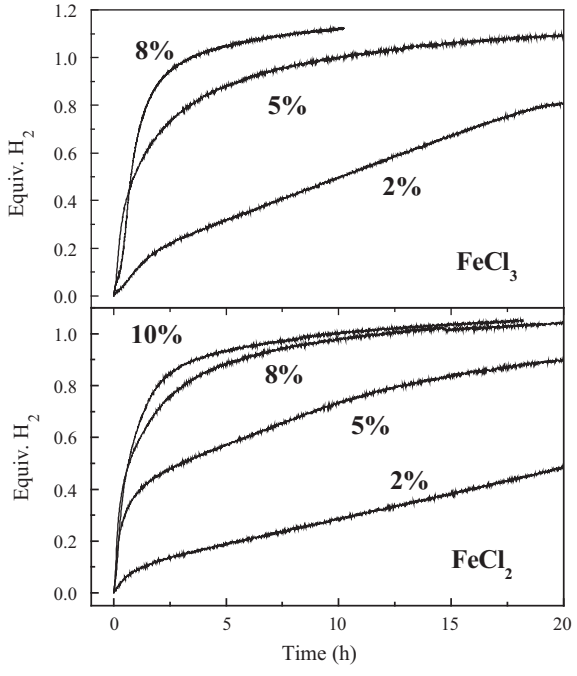

Fig. 3. Volumetric release measurements on $FeCl_2$ and $FeCl_3$-doped AB samples with various loadings at 60 °C.

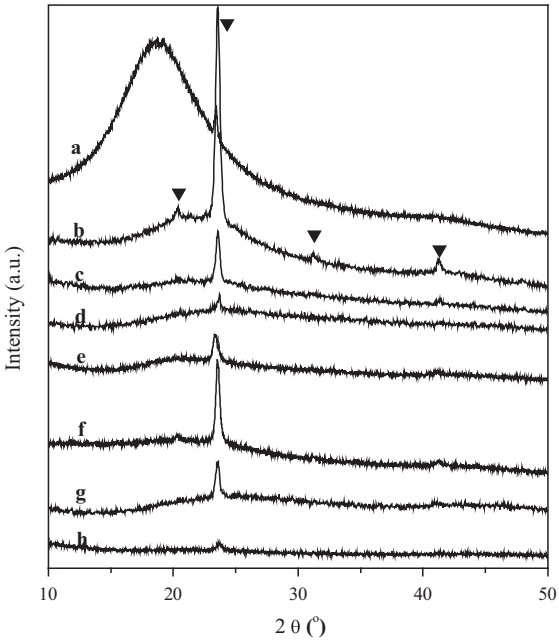

Fig. 4. XRD patterns of post dehydrogenated (a) neat AB at 80 °C; (b–d): 2.0, 5.0 and 8.0% $FeCl_3$-doped AB at 60 °C; and (e–h): 2.0, 5.0, 8.0 and 10.0% $FeCl_2$-doped AB at 60 °C. (▼, crystalline linear PAB).

Fig. 5 shows the FTIR measurement on the post-dehydrogenated 2.0% $FeCl_3$-doped AB sample which is similar to both of the crystalline CPB [32,33] and ordered linear PAB [34]. Due to the existence of iron species in the post-dehydrogenated sample, the low frequency region of FTIR spectrum arises several new peaks. Here, we give a general name, crystalline PAB, to the ordered products from Fe–Based catalytic dehydrogenation of AB. It is worth noting that crystalline PAB can also be obtained through Co- and Ni-based catalytic dehydrogenation of AB. For $FeCl_3$-doped AB samples, 2.0% catalyst loading produces the highest crystallinity of PAB in the post-dehydrogenated samples as shown in Fig. 4. However, the post-dehydrogenated 5.0% $FeCl_2$-doped AB sample exhibits a better crystallinity than 2.0, 8.0 and 10.0% loadings in $FeCl_2$-doped samples. It can be concluded that, to obtain a better crystallinity, the crystal growth rate of PAB should match well with the monomer (NH_2NH_2) formation rate, i.e. dehydrogenation rate of AB. Neither too fast nor too slow dehydrogenation rate of AB is suitable for the growth of crystalline PAB.

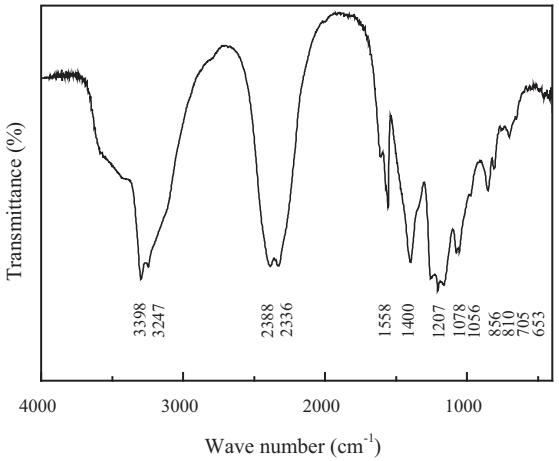

Fig. 5. FTIR spectrum of post-dehydrogenated 2.0% $FeCl_3$-doped AB at 60 °C.

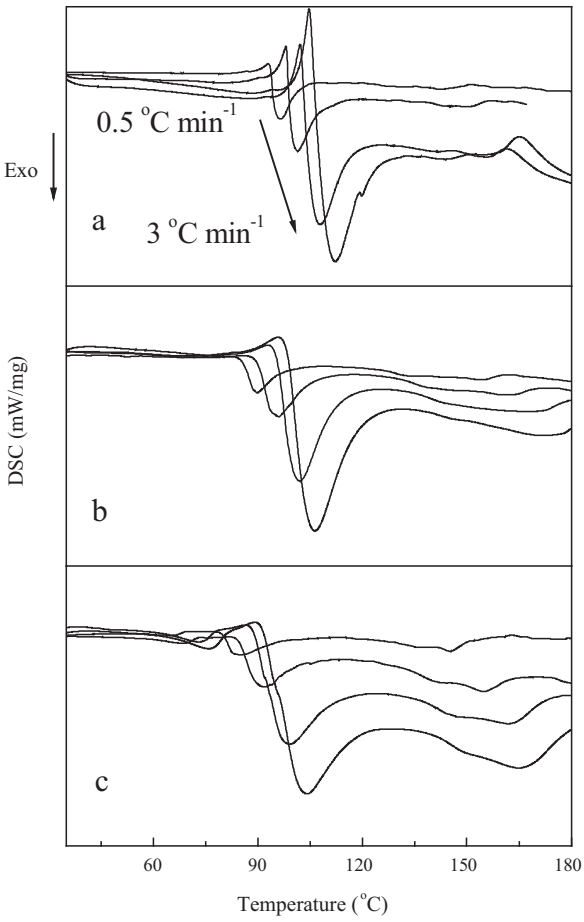

Fig. 6. DSC profiles of dehydrogenation of neat (a), 2.0% $FeCl_2$-doped (b) and 2.0% $FeCl_3$-doped (c) AB samples at heating rates of 0.5, 1, 2, 3 °C min^{-1}, respectively.

Nuclear magnetic resonance (NMR) is a good method to characterize the degree of polymerization of PAB. However, Fe or Fe related species in the dehydrogenated sample became a paramagnetic material. The presence of the paramagnetic iron species in the sample made solid NMR characterization interpretation inclusive, which discouraged our attempt in using NMR to see the ^{11}B chemical environment. Also, the trials on liquid NMR using solvent such as DMSO, H_2O and hydrazine are unsuccessful probably due to the difficulty of removing nanosized catalyst (or maybe some solid product) from the liquid phase.

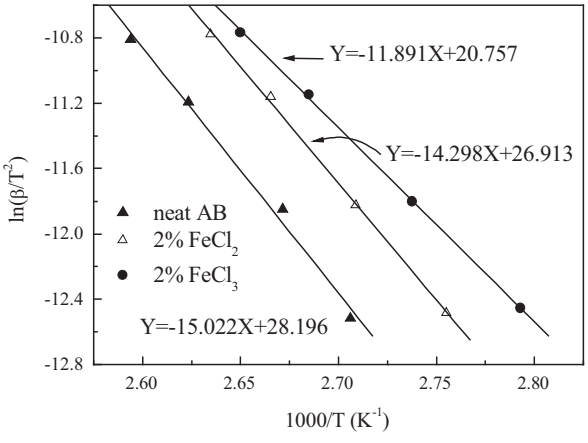

Fig. 7. Kissinger plots of the neat (▲), 2.0% $FeCl_2$-doped (△) and 2.0% $FeCl_3$-doped (●) AB samples at different heating rates.

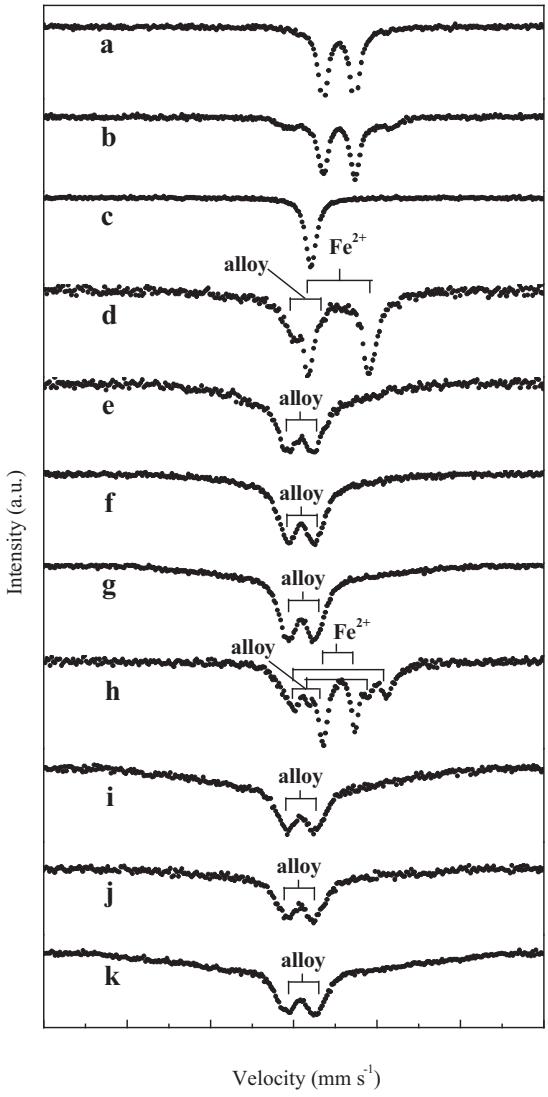

Fig. 8. Quasi in situ ^{57}Fe Mössbauer spectra of (a) $FeCl_2$, (b) $FeCl_2$ distilled from THF, (c) $FeCl_3$, and (d–g) 5.0% $FeCl_3$-doped AB samples dehydrogenated 0, 0.2, 0.6 and 1.2 equiv. H_2 at 80 °C; (h–k) 5.0% $FeCl_2$-doped AB samples dehydrogenated 0, 0.2, 0.6 and 1.2 equiv. H_2 at 80 °C.

3.3. Kinetic analysis

To gain the insight of the enhanced kinetics, the reaction kinetic parameters (activation energy E_a and the pre-exponential factor A) are determined using the Kissinger equation [35–37], namely:

$$\ln\left(\frac{\beta}{T_p^2}\right) = \ln\left(\frac{AR}{E_a}\right) - \frac{E_a}{RT_p} \quad (1)$$

Here T_p is the temperature at which the maximum reaction rate peaks, A is the pre-exponential factor, β is the heating rate, E_a is the activation energy and R is the gas constant. The temperature of maximum reaction rate at different heating rates is determined by DSC technique (shown in Fig. 6). The dependence of $\ln(\beta/T_p^2)$ vs. $1/T_p$ is plotted in Fig. 7. The activation energy E_a and the pre-exponential factor A are calculated from the slope ($-E_a/R$) and the intercept ($\ln(AR/E_a)$) of the fitted line, respectively. Once E_a and A are known, the specific rate constant k at a given temperature can

Table 2
^{57}Fe Mössbauer parameters of 5.0 mol.% $FeCl_2$ and $FeCl_3$-doped AB samples dehydrogenated 0, 0.2, 0.6 and 1.2 equiv. H_2 at 80 °C. For comparison, parameters of pristine $FeCl_2$, $FeCl_3$ and $FeCl_2$ distilled from THF are also listed.

Composition	Oxidation state of Fe	IS[a] ($mm\,s^{-1}$)	QS[b] ($mm\,s^{-1}$)	Average magnetic field (T)	Spectral area (%)[c]	FWHM[d] ($mm\,s^{-1}$)
$FeCl_2$ in Ar (a)	Fe^{2+}	1.09	0.76	–	100	0.28
$FeCl_2$ from THF (b)	Fe^{2+}	1.09	0.77	–	73	0.28
	Fe^{2+}	1.08	2.35	–	27	0.62
$FeCl_3$ in Ar (c)	Fe^{3+}	0.42	–	–	100	0.30
AB + 5%$FeCl_3$ (d)	Fe^{2+}	1.08	1.50	–	84	0.40
	Alloy	0.20	–	26.3	16	0.30
AB + 5%$FeCl_3$ − 0.2H_2 (e)	Alloy	0.19	–	20.5	100	0.28
AB + 5%$FeCl_3$ − 0.6H_2 (f)	Alloy	0.19	–	16.1	100	0.21
AB + 5%$FeCl_3$ − 1.2H_2 (g)	Alloy	0.20	–	15.2	100	0.22
AB + 5%$FeCl_2$ (h)	Fe^{2+}	1.09	0.77	–	35	0.25
	Fe^{2+}	1.13	2.22	–	32	0.37
	Fe^{2+}	1.08	1.43	–	10	0.29
	Alloy	0.19	–	27.4	23	0.20
AB + 5%$FeCl_2$ − 0.2H_2 (i)	Alloy	0.19	–	17.3	100	0.29
AB + 5%$FeCl_2$ − 0.6H_2 (j)	Alloy	0.18	–	17.8	100	0.24
AB + 5%$FeCl_2$ − 1.2H_2 (k)	Alloy	0.18	–	17.5	100	0.29

[a] IS, isomer shift, relative to α-Fe at room temperature.
[b] QS, electric quadrupole splitting.
[c] Relative resonance areas of the different components of the absorption patterns.
[d] Full line width at half maximum: uncertainty is ±5% of the reported values.

be determined by the Arrhenius equation:

$$k = A\ \exp\left(\frac{-E_a}{RT}\right) \quad (2)$$

Table 1 presents E_a, A and k (at 60 °C) for each sample. As mentioned above, the rate constant k at 60 °C of $FeCl_3$-doped AB is larger than $FeCl_2$-doped and pristine AB which agrees with the order of hydrogen releasing rate determined in volumetric release measurements. The E_a of the first dehydrogenation step of $FeCl_3$-doped AB is reduced to 98.8 kJ mol^{-1}, and the rate constant k of 2.0% $FeCl_3$-doped AB system is 5.8 times as that of the neat AB at 60 °C.

3.4. Quasi in situ ^{57}Fe Mössbauer investigations

Mössbauer technique is an effective way to identify the catalyst components in terms of active phase or active sites [38,39], especially on the amorphous materials, i.e. the short-range order and long-range disorder in structure [40–42]. Since the amorphous state of Fe species in our samples, quasi in situ ^{57}Fe Mössbauer spectroscopy were employed to identify the changes of chemical state and local environment of Fe during dehydrogenation process as shown in Fig. 8. The 5.0% Fe–Based catalyst loading sample was characterized by ^{57}Fe Mössbauer technique in order to shorten signal accumulation time. 1.2 equiv. H_2 can be released from 5.0% Fe–Based catalyst loading AB at 80 °C in 40 h. For a comparison, pristine $FeCl_2$ (Fig. 8a) and $FeCl_3$ (Fig. 8c) were also characterized by ^{57}Fe Mössbauer spectroscopy. Corresponding evaluated ^{57}Fe Mössbauer parameters are exhibited in Table 2. The IS values of $FeCl_2$ and $FeCl_3$ are 1.09 and 0.42 $mm\,s^{-1}$, respectively, which are consistent with Ref. [43]. Spectrum of Fig. 8b is $FeCl_2$ distilled from a mixture of $FeCl_2$ and THF. We can see that, besides pristine $FeCl_2$, there is a new ferrous quadrupole doublet which is reasonably attributed to $FeCl_2$ adducted with THF like $FeCl_2$ adducted with H_2O in the literature [43,44]. The Mössbauer spectrum for the as-prepared $FeCl_3$-doped AB sample mainly contains one ferrous quadrupole doublet and one alloyed iron with a distribution in hyperfine magnetic field (Fig. 8d), showing the reduction of Fe^{3+} to Fe^{2+} and alloyed state by AB upon mixing $FeCl_3$ and AB at ambient temperature. However, for the as-prepared $FeCl_2$-doped AB, the spectrum is consisted of three ferrous quadrupole doublets and an alloyed component with a distribution in hyperfine magnetic field (Fig. 8h), showing that partial reaction of $FeCl_2$ with AB upon mixing them at ambient temperature. The alloyed component in $FeCl_3$ and $FeCl_2$-doped AB keeps unchanged and functions as active center during the catalytic dehydrogenation of AB which will be discussed below. The IS at 1.09 and 1.13 $mm\,s^{-1}$ with electric quadrupole splitting (QS) at 0.77 and 2.22 $mm\,s^{-1}$ should belong to pristine $FeCl_2$ (Fig. 8a) and $FeCl_2$ adducted with THF as mentioned above in Fig. 8b, respectively. These two species (account 67%) do not have interaction with AB, indicting worse dispersion of $FeCl_2$ on AB, which is consistent with lower catalytic activity of $FeCl_2$ than that of $FeCl_3$ as mentioned above. The residue Fe^{2+} species with IS at 1.08 $mm\,s^{-1}$ and QS at 1.43 $mm\,s^{-1}$ is similar with Fe^{2+} in the as-prepared $FeCl_3$-doped AB, showing the formation of same species between AB and $FeCl_2$ or $FeCl_3$ at ambient temperature. As illustrated in Section 3.2, 2.0 mol.% $FeCl_3$ loading exhibited the best crystallinity of PAB. However, the dispersion of $FeCl_2$ on AB is worse than that of $FeCl_3$, indicating that more $FeCl_2$ are needed to perform a similar catalytic activity and crystallinity of PAB. Thus, for $FeCl_2$-doped AB sample, 5.0 mol.% loading gave the best performance in the formation of crystalline PAB. In our previously report, FeB nanoalloys were identified as functional species in the post-dehydrogenated Fe–Based catalyst loading AB sample [1]. However, changes of Fe chemical state during the dehydrogenation process were not studied in details. Thus, to gain insight into the dehydrogenation process, samples at different dehydrogenated stages are collected for quasi in situ ^{57}Fe Mössbauer characterization. As shown in Fig. 8e–g and i–k, when the $FeCl_3$- and $FeCl_2$-doped AB samples are heated to 80 °C and released 0.2, 0.6 and 1.2 equiv. H_2, respectively, identical patterns with an average isomer shift around 0.19 $mm\,s^{-1}$ relative to α-iron were observed, which is similar to the isomer shift (0.19 $mm\,s^{-1}$) of $Fe_{44}Co_{19}B_{37}$ and $Fe_{62}B_{38}$ amorphous alloys reported by van Wonterghem et al. [40] We can conclude that all the Fe^{2+} species is reduced to Fe–B alloy upon heating the samples to higher temperature in which the Fe–B alloy keeps unchanged and functions as catalyst in the following dehydrogenation process.

3.5. XAS investigation

More information regarding the chemical state and local structures of Fe in the post-dehydrogenated $FeCl_2$- and $FeCl_3$-doped AB samples is obtained from the XAS analysis. Fe foil, $FeCl_2$ and $FeCl_3$ are also used as reference samples. As shown in Fig. 9, the Fe K-edge X-ray absorption near edge structure (XANES) spectra of

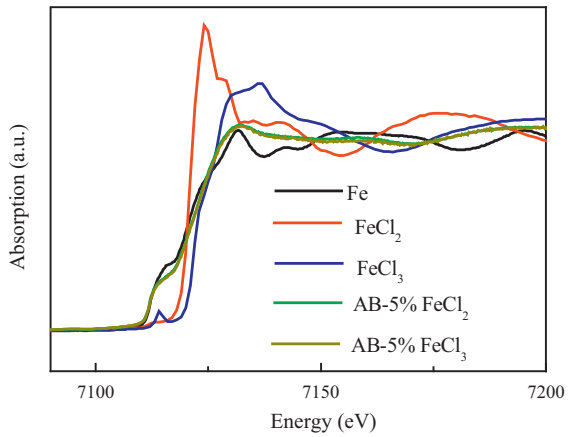

Fig. 9. Fe K-edge XANES spectra of metallic Fe, $FeCl_2$, $FeCl_3$ and post-dehydrogenated 5.0 mol.% $FeCl_2$- or $FeCl_3$-doped AB samples.

the post-dehydrogenated $FeCl_2$- and $FeCl_3$-doped AB samples are much similar with each other which resemble that of metallic Fe, indicating a zero valence of Fe in post-dehydrogenated samples. However, the Fourier transformed (Fig. 10) pattern of the post-dehydrogenated Fe-doped AB is different from that of the Fe foil. Since ferric or ferrous salts are easy to be reduced by BH_4^- and alloy with B to form amorphous Fe–B alloys in solution [40,42], $FeCl_2$ in the sample may be reduced and alloy with B in AB during sample preparation and dehydrogenation treatment, which is confirmed by previous report [1] and Mössbauer characterization as mentioned above. The post-dehydrogenated sample shows a much broadened peak with the absence of high-order coordination peaks indicating an amorphous state of Fe species consistent with XRD results. The broadened peak attributes to the overlap of Fe–B and Fe–Fe coordination at the first and the second shells [45]. Because of the small X-ray scattering power for B, the Fe–B coordination peak is weak and overlapped with Fe–Fe. Quantitative information of local structural parameters was obtained by fitting of the first peak in real space using the phase shift and backscattering amplitude extracted from theoretical FeB compound. The single scattering paths of Fe–B and Fe–Fe were included in the fitting; the inelastic factor was fixed to 0.9. A reasonable fit of the first peak gives a Fe–B and Fe–Fe bond length of 2.12 and 2.50 Å, respectively. Table 3 presents the structure parameters of post-dehydrogenated 5.0% $FeCl_2$-doped AB sample. The distances of Fe–B and Fe–Fe in

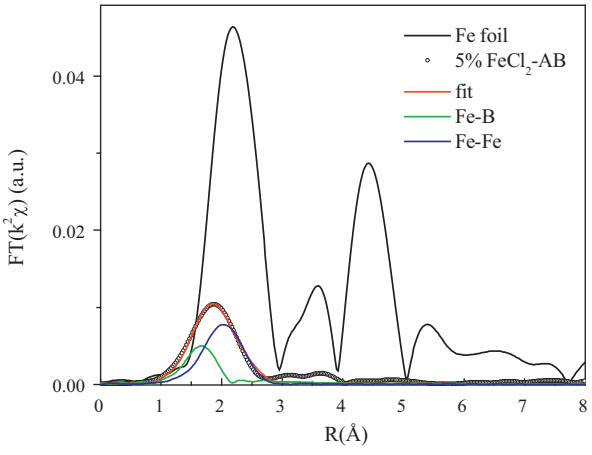

Fig. 10. Fourier transform of Fe K-edge EXAFS of Fe foil and post-dehydrogenated 5.0% $FeCl_2$-doped AB sample, the latter was fitted with Fe–B and Fe–Fe coordination. Phase shifts were not corrected.

Table 3
Structural parameters from EXAFS on Fe K edge of post-dehydrogenated 5% $FeCl_2$-doped AB. The values in parentheses show the estimated errors.

Sample	Pair	*N*	*R* (Å)	σ^2 (Å^2)
5% $FeCl_2$–AB	Fe–B	2.0(0.2)	2.12(0.01)	0.001(0.0002)
	Fe–Fe	2.8(0.3)	2.50(0.02)	0.011(0.002)

the first and second shells are close to the FeB from PDFs [1] and supports the formation of FeB alloy (1.73–2.16 Å) [40,41]. Here, we can conclude most likely that Fe forms solid solution alloy with B as reported. Since the formation of ordered PAB, the polymerization may follow the Ziegler–Natta mechanism [46–48] accompanied with dehydrogenation in which Fe–B alloy functions as active center.

4. Conclusions

Approximately 1 equiv. H_2 can be released from 2.0 mol.% $FeCl_2$- and $FeCl_3$-doped AB at a temperature as low as 60 °C with significantly depression of induction period, sample foaming and toxic byproducts (borazine and NH_3). $FeCl_3$-modifyed AB exhibited superior performance than $FeCl_2$-modified sample. Crystalline PAB is formed from the dehydrogenation of Fe-doped AB, in which Fe–B alloy is identified as the functional species during the catalytic dehydrogenation.

Acknowledgements

This work is supported by Hundred Talents Project (KGCX2-YW-806), Knowledge Innovation Program of CAS (KJCX2-YW-H21), 863 (2009AA05Z108) Project, 973 (2010CB631304) Project and National Natural Science Foundation of China (Nos. 20971120, 10979051, 20973162 and 11079036).

Appendix A. Supplementary data

Supplementary data associated with this article can be found, in the online version, at doi:10.1016/j.cattod.2011.02.041.

References

[1] T. He, J. Wang, G. Wu, H. Kim, Th. Proffen, A. Wu, W. Li, T. Liu, Z. Xiong, C. Wu, H. Chu, J. Guo, T. Autrey, T. Zhang, P. Chen, Chem. Eur. J. 16 (2010) 12814–12817.
[2] L. Schlapbach, A. Züttel, Nature 414 (2001) 353–358.
[3] S.-i. Orimo, Y. Nakamori, J.R. Eliseo, A. Züttel, C.M. Jensen, Chem. Rev. 107 (2007) 4111–4132.
[4] F.H. Stephens, V. Pons, R.T. Baker, J. Chem. Soc. Dalton Trans. (2007) 2613–2626.
[5] C.W. Hamilton, R.T. Baker, A. Staubitz, I. Manners, Chem. Soc. Rev. 38 (2009) 279–293.
[6] M.G. Hu, R.A. Geanangel, W.W. Wendlandt, Thermochim. Acta 23 (1978) 249–255.
[7] F. Baitalow, J. Baumann, G. Wolf, K. Jaenicke-Rößler, G. Leitner, Thermochim. Acta 391 (2002) 159–168.
[8] G. Wolf, J. Baumann, F. Baitalow, F.P. Hoffmann, Thermochim. Acta 343 (2000) 19–25.
[9] A. Gutowska, L. Li, Y. Shin, C.M. Wang, X.S. Li, J.C. Linehan, R.S. Smith, B.D. Kay, B. Schmid, W. Shaw, M. Gutowski, T. Autrey, Angew. Chem. Int. Ed. 44 (2005) 3578–3582.
[10] A. Feaver, S. Sepehri, P. Shamberger, A. Stowe, T. Autrey, G. Cao, J. Phys. Chem. B 111 (2007) 7469–7472.
[11] D. Neiner, A. Karkamkar, J.C. Linehan, B. Arey, T. Autrey, S.M. Kauzlarich, J. Phys. Chem. C 113 (2008) 1098–1103.
[12] M.C. Denney, V. Pons, T.J. Hebden, D.M. Heinekey, K.I. Goldberg, J. Am. Chem. Soc. 128 (2006) 12048–12049.
[13] R.J. Keaton, J.M. Blacquiere, R.T. Baker, J. Am. Chem. Soc. 129 (2007) 1844–1845.
[14] F.H. Stephens, R.T. Baker, M.H. Matus, D.J. Grant, D.A. Dixon, Angew. Chem. Int. Ed. 46 (2007) 746–749.
[15] D.W. Himmelberger, C.W. Yoon, M.E. Bluhm, P.J. Carroll, L.G. Sneddon, J. Am. Chem. Soc. 131 (2009) 14101–14110.
[16] M. Käß, A. Friedrich, M. Drees, S. Schneider, Angew. Chem. Int. Ed. 48 (2009) 905–907.
[17] M.E. Bluhm, M.G. Bradley, R. Butterick, U. Kusari, L.G. Sneddon, J. Am. Chem. Soc. 128 (2006) 7748–7749.

[18] D.W. Himmelberger, L.R. Alden, M.E. Bluhm, L.G. Sneddon, Inorg. Chem. 48 (2009) 9883–9889.
[19] Z. Xiong, C.K. Yong, G. Wu, P. Chen, W. Shaw, A. Karkamkar, T. Autrey, M.O. Jones, S.R. Johnson, P.P. Edwards, W.I.F. David, Nat. Mater. 7 (2008) 138–141.
[20] H.V.K. Diyabalanage, R.P. Shrestha, T.A. Semelsberger, B.L. Scott, M.E. Bowden, B.L. Davis, A.K. Burrell, Angew. Chem. Int. Ed. 46 (2007) 8995–8997.
[21] Z. Xiong, Y.S. Chua, G. Wu, W. Xu, P. Chen, W. Shaw, A. Karkamkar, J. Linehan, T. Smurthwaite, T. Autrey, Chem. Commun. (2008) 5595–5597.
[22] H. Wu, W. Zhou, T. Yildirim, J. Am. Chem. Soc. 130 (2008) 14834–14839.
[23] J. Spielmann, G. Jansen, H. Bandmann, S. Harder, Angew. Chem. Int. Ed. 120 (2008) 6386–6391.
[24] Z. Xiong, G. Wu, Y.S. Chua, J. Hu, T. He, W. Xu, P. Chen, Energy Environ. Sci. 1 (2008) 360–363.
[25] C. Wu, G. Wu, Z. Xiong, X. Han, H. Chu, T. He, P. Chen, Chem. Mater. 22 (2009) 3–5.
[26] Y.S. Chua, G. Wu, Z. Xiong, T. He, P. Chen, Chem. Mater. 21 (2009) 4899–4904.
[27] T. He, Z. Xiong, G. Wu, H. Chu, C. Wu, T. Zhang, P. Chen, Chem. Mater. 21 (2009) 2315–2318.
[28] T. Ressler, J. Phys. IV France 7 (1997), C2-269-C262-270.
[29] A.C. Stowe, W.J. Shaw, J.C. Linehan, B. Schmid, T. Autrey, Phys. Chem. Chem. Phys. 9 (2007) 1831–1836.
[30] D.J. Heldebrant, A. Karkamkar, N.J. Hess, M. Bowden, S. Rassat, F. Zheng, K. Rappe, T. Autrey, Chem. Mater. 20 (2008) 5332–5336.
[31] W.J. Shaw, J.C. Linehan, N.K. Szymczak, D. Heldebrant, C. Yonker, D. Camaioni, R.T. Baker, T. Autrey, Angew. Chem. Int. Ed. 47 (2008) 7493–7496.
[32] K.W. Böddeker, S.G. Shore, R.K. Bunting, J. Am. Chem. Soc. 88 (1966) 4396–4401.
[33] http://www.hydrogen.energy.gov/pdfs/review06/st_4_heinekey.pdf.
[34] A. Staubitz, A.P. Soto, I. Manners, Angew. Chem. Int. 47 (2008) 6212–6215.
[35] H.E. Kissinger, Anal. Chem. 29 (1957) 1702–1706.
[36] T. Ozawa, J. Therm. Anal. Calorim. 2 (1970) 301–324.
[37] J.A.F.F. Rocco, J.E.S. Lima, A.G. Frutuoso, K. Iha, M. Ionashiro, J.R. Matos, M.E.V. Suárez-Iha, J. Therm. Anal. Calorim. 75 (2004) 551–557.
[38] J. Wang, K. Ozawa, M. Takahashi, M. Takeda, T. Nonami, Chem. Mater. 18 (2006) 2261–2264.
[39] A. Fukuoka, T. Kimura, N. Kosugi, H. Kuroda, Y. Minai, Y. Sakai, T. Tominaga, M. Ichikawa, J. Catal. 126 (1990) 434–450.
[40] J. van Wonterghem, S. Mørup, C.J.W. Koch, S.W. Charles, S. Wells, Nature 322 (1986) 622–623.
[41] S. Linderoth, J. Magn. Magn. Mater. 104–107 (1992) 128–130.
[42] S. Linderoth, S. Møup, A. Meagher, J. Larsen, M.D. Bentzon, B.S. Clausen, C.J.W. Koch, S. Wells, S.W. Charles, J. Magn. Magn. Mater. 81 (1989) 138–146.
[43] H. Sano, M. Katada, Mössbauer Spectroscopy (Fundamentals and Application), Gakkai Publication Center, 1996 (in Japanese).
[44] N.N. Greenwood, T.C. Gibb, Mössbauer Spectroscopy, Chapaman and Hall Ltd., London, 1971.
[45] S.B. Qadri, M.A. Dinderman, W.J. Dressick, P.E. Schoen, P. Lubitz, J.H. He, R.J. Tonucci, J. Cross, Appl. Phys. A 89 (2007) 493–496.
[46] P. Cossee, J. Catal. 3 (1964) 80–88.
[47] E.J. Arlman, J. Catal. 3 (1964) 89–98.
[48] E.J. Arlman, P. Cossee, J. Catal. 3 (1964) 99–104.